Eur. Phys. J. B **9**, 83–91 (1999)

THE EUROPEAN PHYSICAL JOURNAL B

EDP Sciences
© Società Italiana di Fisica
Springer-Verlag 1999

Characterization of the structure and the size distribution of branched polymers formed by co-polymerization of MMA and EGDMA

V. Lesturgeon, D. Durand, and T. Nicolai[a]

Chimie et Physique des Matériaux Polymères[b], Université du Maine, 72085 Le Mans Cedex 9, France

Received 11 May 1998 and Received in final form 22 October 1998

Abstract. Free radical co-polymerization of methyl methacrylate (MMA) and ethyl glycol dimethyl methacrylate (EGDMA) in solution leads to the formation of polydisperse branched PMMA which grows in size until the system gels. The structure and the size distribution of the PMMA aggregates were characterized at infinite dilution using static and dynamic light scattering and size exclusion chromatography (SEC). The reaction extent was measured using SEC and Raman spectroscopy. The results show that the structure and size distribution of PMMA aggregates formed close to the gel point are compatible with those of percolating clusters. The structure factor of semi-dilute solutions of PMMA aggregates is the same as that of dilute solutions at distance scales much smaller than the correlation length of the concentration fluctuations (ξ). However, the cut-off function of the pair correlation function at ξ for semi-dilute solutions is more gradual than the cut-off function at $R_{\rm gz}$ for dilute solutions.

PACS. 36.20.-r Macromolecules and polymer molecules – 61.10.-i X-ray diffraction and scattering

1 Introduction

For a good understanding of the properties of gels and the process of the gel formation, it is necessary to know the structure and size distribution of the particles that are formed before the gel point. A multitude of different types of gels have been investigated as distinct as egg white formed by aggregating globular proteins and rubber formed by cross-linking long flexible chains. In spite of the large variety a common model, three-dimensional percolation, has been proposed to describe the structural features of the gel formation very close to the gel point [1]. The justification for this model is that the sol-gel transition is a critical phenomenon, which is independent of the specific properties of the elementary units of the gel. Properties such as functionality, reactivity and rigidity only determine the kinetics and local structure. The universal percolation process is postulated to start once the aggregates, *e.g.* branched polymers, are very large compared to the elementary unit and together fill up the whole space. In theory this process only occurs infinitesimally close to the gel point. Properties of the percolation process are often expressed in terms of $\varepsilon = |P_{\rm c} - P|/P_{\rm c}$ which expresses the approach of the system to the gel point [2]. In Monte-Carlo simulations P can be the number of sites or bonds, while experimentally parameters like the reaction extent, reaction time or relative amount of cross-linker have been used. $P_{\rm c}$ is the critical value at the gel point. It is clear that the value of $P_{\rm c}$ is not universal, but that it depends on the system or the type of Monte-Carlo simulation. However, scaling laws such as the one that describes the divergence of the z-average radius of gyration ($R_{\rm gz}$) as $\varepsilon \to 0$ are independent of the choice of P and the value of $P_{\rm c}$.

However important from a theoretical point of view, the percolation model is of little use for the study of gels if not applicable at some distance away from the gel point. The minimum size of the aggregates beyond which they show the characteristics of percolating clusters varies from system to system. On smaller size scales different aggregation models can be useful, *e.g.* mean field theory in the case of monomers with known functionality [3], or flocculation models in the case of colloidal aggregation [4]. Large crossover domains can be expected so often no model applies. Nevertheless, the percolation model has given a good description of structural properties of the aggregates in a number systems [5–8].

The percolation model only gives structural properties and has to be supplemented to give predictions for mechanical and other dynamical properties. In this way the gel modulus has been calculated for flexible polymer gels assuming that the gel fraction is a homogeneous three dimensional network. The viscosity and the frequency dependence of the elastic modulus have been calculated assuming normal modes relaxation of the aggregates [9]. Whatever the additional assumptions, these theories

[a] e-mail: nicolai@univ-lemans.fr
[b] UMR CNRS

presuppose a particular structure and size distribution of the aggregates which is provided by the percolation model.

Elsewhere [10] we have reported a study of free radical copolymerization of methyl methacrylate (MMA) in the presence of various quantities of ethylene glycol dimethacrylate (EGDMA). We have investigated the gel formation in situ using static (SLS) and dynamic (DLS) light scattering. We have also studied the effect of progressive dilution on a quenched system close to the gel point. The experimental results could be interpreted assuming that percolation clusters are formed and that hydrodynamic interaction is screened.

Here we present a detailed characterization of the aggregates at infinite dilution. For one system the characterization of the size distribution was reported in reference [11] using size exclusion chromatography with on-line SLS, refractive index and viscosity detection. We will show that initially linear PMMA chains are formed which subsequently cross-link to form self-similar flexible aggregates. Both the size distribution and the structure is compatible with those of percolating clusters independent of the amount of EGDMA in the range investigated ($0.05 \geq$ [EGDMA]/[MMA] ≥ 0.005). The present results together with those reported in reference [11] justify the use of the percolation model in reference [10].

2 Experimental

2.1 Sample preparation

Solutions were prepared by dissolving the required amounts of MMA and EGDMA (Merck) in freshly distilled toluene. 1.1×10^{-3} g/ml AIBN was added to initialize the reaction. The solutions were filtered through 0.2 μm pore size Anotop filters. Free radical polymerization was done at 68 ± 0.1 °C during set reaction times after which the reaction was quenched by rapid cooling. The solutions were diluted in THF by more than a factor 1000. In one case the reaction was done in THF and the effect of progressive dilution was investigated.

2.2 Light scattering

Static and dynamic light scattering measurements were made at 20 ± 0.1 °C using an ALV-5000 multi-bit multi-tau correlator in combination with a Malvern goniometer and a Spectra Physics argon ion laser operating with vertically polarized light with wave lengths $\lambda = 488$ nm or 514.5 nm. The measurements were done over a range of scattering angles: $13 \leq \theta \leq 150$. The corresponding range of the scattering wave vectors ($q = (4\pi n_s/\lambda)\sin(\theta/2)$, with n_s the solvent refractive index) is between 4×10^{-3} and 4×10^{-2} nm^{-1}. The scattering contrast factor K was determined using a toluene standard [12]:

$$K = \frac{4\pi^2 {n_s}^2}{\lambda^4 N_a} \left(\frac{\partial n}{\partial C}\right)^2 \left(\frac{n_{tol}}{n_s}\right)^2 \frac{I_{tol}}{R_{tol}}.$$

Here N_a is Avogadro's number, $(\partial n/\partial C) = 0.089$ ml/g [13] is the refractive index increment of PMMA in THF, and R_{tol} is the Rayleigh factor of toluene at 20 °C (4.0×10^{-5} and 3.3×10^{-5} cm^{-1} at $\lambda = 488$ nm and 514.5 nm, respectively [14]). $(n_{tol}/n_s)^2$ corrects for the difference in scattering volume of the solution and the toluene standard.

2.3 Size exclusion chromatography (SEC)

Two PL-Gel columns (Polymer Laboratories, type "Mixed" and "Mixed B") were used in series. The eluant was THF and the flow rate 1 cm^3/min. The concentration was monitored by a differential refractometer (R410 from Millipore-Waters).

2.4 Raman spectroscopy

Raman spectra were recorded in the classical 90° configuration with a DILOR Z-24 single-channel trippel monochromator equipped with a cooled photomultiplier. The spectra were recorded by counting for 1 s at 0.5 cm^{-1} intervals between 1530 and 1680 cm^{-1}. The exiting source was a Coherent Innova 90.3 argon ion laser; 514.5 nm excitation radiation was selected with an incident power of 150 mW.

3 Theory

For a recent review of the theory of SLS and DLS on dilute solutions of polydisperse fractal aggregates see reference [15]. Here we will briefly summarize the expressions that are needed to interpret our experimental results.

For different types of aggregation the number of aggregates with molar mass ($N(M)$) has a power law dependence:

$$N(M) \propto M^{-\tau} f(M/M^*) \qquad M \gg M_0 \qquad (1)$$

with M_0 the molar mass of the smallest particle in the distribution and $f(M/M^*)$ a cut-off function at a characteristic molar mass M^* which decreases faster than any power law. For aggregates with a fractal structure the pair correlation function is:

$$g(r) \propto r^{d_f - 3} f(r/R_g) \qquad r \gg r_0 \qquad (2)$$

with d_f the so-called fractal dimension, r_0 the size of the elementary unit and $f(r/R_g)$ another cut-off function. It follows from equation (2) that the molar mass scales with the radius of gyration: $M \propto R_g^{d_f}$. Monte-Carlo simulations of $3d$ percolation give $d_f = 2.5$ and $\tau = 2.2$ [2]. However, d_f is smaller if flexible aggregates are diluted because excluded volume interactions are no longer screened so that the aggregates swell. A mean field argument gives $d_f = 2.0$ for flexible percolating clusters in a good solvent [16].

To calculate the scattering intensity by a dilute solution of polydisperse aggregates we need the z-average pair correlation function:

$$g_z(r) \propto r^{d_f^* - 3} f(r/R_{gz}) \qquad r \gg r_0. \tag{3}$$

d_f^* is an effective fractal dimension related to d_f *via* the polydispersity exponent τ:

$$\begin{aligned} d_f^* &= d_f(3-\tau) \quad \tau > 2, \\ d_f^* &= d_f \qquad\qquad \tau < 2. \end{aligned} \tag{4}$$

$f(r/R_{gz})$ is an effective cut-off function at the z-average radius of gyration and depends on the cut-off functions in equations (1, 2).

The time average intensity scattered by the aggregates, *i.e.* the total scattering minus the scattering by the solvent ($I = I_{tot} - I_{sol}$), is given by:

$$I = KCM_w S_z(q). \tag{5}$$

Here K is a contrast factor (see Sect. 2), C is the aggregate concentration, M_w is the weight average molar mass and $S_z(q)$ is the z-average structure factor. For highly diluted solutions inter particle interference is negligible and $S_z(q)$ can be calculated by taking the Fourier transform of $g_z(r)$. The general form of $S_z(q)$ depends on the choice of the cut-off functions, but has the following limiting behaviour independent of the cut-off functions:

$$S_z(q) = \left[1 + \frac{1}{3}(qR_{gz})^2\right]^{-1} \qquad qR_{gz} < 1 \tag{6}$$

$$S_z(q) = a_1 (qR_{gz})^{-d_f^*} \qquad r_0 \ll q^{-1} \ll R_{gz} \tag{7}$$

where a_1 is a constant which depends on the cut-off functions. d_f^* can thus be determined by measuring the q-dependence of the scattered intensity:

$$\frac{I}{KC} = a_2 q^{-d_f^*} \qquad r_0 \ll q^{-1} \ll R_{gz} \tag{8}$$

where a_2 is another constant which depends on the local structure of the aggregates. Alternatively, d_f^* can be determined from the relation between R_{gz} and M_w:

$$M_w = a_3 R_{gz}^{d_f^*} \qquad M_w \gg M_0. \tag{9}$$

From equations (5, 7–9) it follows that a_3 is related to a_1 and a_2: $a_3 = a_2/a_1$.

With DLS the intensity autocorrelation function is measured. If the scattered light has Gaussian statistics the normalized intensity autocorrelation function ($g_2(t)$) is related to the normalized electric field autocorrelation function ($g_1(t)$) as [17]: $g_2(t) = 1 + g_1(t)^2$. The excess scattered light is due to concentration fluctuations of the aggregates. For dilute solutions of monodisperse particles with $qR_g < 1$, $g_1(t)$ is a single exponential decay with relaxation time $\tau = (q^2 D)^{-1}$, with D the translational diffusion coefficient. D is related to the hydrodynamic radius R_h *via* the so-called Stokes-Einstein relation:

$$D = \frac{k_B T}{6\pi\eta R_h} \tag{10}$$

with k_B Boltzmann's constant, T the absolute temperature and η the solvent viscosity. For polydisperse dilute solutions $g_1(t)$ is characterized by a distribution of relaxation times ($A(\tau)$):

$$g_1(t) = \int A(\log\tau)\, \exp(-t/\tau) \mathrm{d}\log\tau. \tag{11}$$

We express the relaxation time distribution as a function of $\log\tau$ because $g_1(t)$ is determined on a logarithmic time scale. The contribution to the scattering of the aggregates is proportional to the square of their molar mass so that:

$$\begin{aligned} A(\log\tau)\mathrm{d}\log\tau \;&\propto\; M^3 N(M)\mathrm{d}\log M \\ \tau \gg \tau_0 \text{ and } qR_g &\ll 1 \end{aligned} \tag{12}$$

with τ_0 the relaxation time which characterizes the diffusion of the smallest particles in the distribution. The z-average diffusion coefficient (D_z) can be obtained by taking the harmonic average of the relaxation time:

$$\langle\Gamma\rangle = \int \tau^{-1} A(\log\tau)\mathrm{d}\log\tau. \tag{13}$$

Alternatively, one can calculate the arithmetic average:

$$\langle\tau\rangle = \int \tau A(\log\tau)\mathrm{d}\log\tau. \tag{14}$$

If $g_1(t)$ is a single exponential decay then the product of the two averages is unity: $\langle\Gamma\rangle\cdot\langle\tau\rangle = 1$. $\langle\Gamma\rangle\cdot\langle\tau\rangle$ can be used as a parameter to characterize the dynamic polydispersity. In very dilute solutions it is directly related to the size polydispersity of the sample.

If $qR_g > 1$ we have to consider the effect of rotational diffusion and internal dynamics which leads to a broadening of the relaxation time distribution even for monodisperse particles. The q-dependence of $\langle\Gamma\rangle$ at large values of qR_g is different for rigid particles: $\langle\Gamma\rangle \propto q^2$, and flexible particles: $\langle\Gamma\rangle \propto q^3$, where we have assumed non-draining in the latter case. However, strong polydispersity influences the q-dependence. If the polydispersity index τ is larger than 2 then $\langle\Gamma\rangle \propto q^3$ both for rigid and flexible particles. Interestingly, for rigid particles the arithmetic average has a weaker than q^3-dependence as long as $\tau < (2 + 1/d_f)$ [18]. This means that for rigid percolating clusters $\langle\Gamma\rangle \cdot \langle\tau\rangle$ continues to increase with q. For flexible percolating clusters $\langle\tau\rangle \propto q^{-3}$ so that $\langle\Gamma\rangle \cdot \langle\tau\rangle$ becomes constant for $qR_{gz} \gg 1$.

4 Results

We studied dilute solutions of PMMA aggregates obtained by co-polymerization of MMA and EGDMA in toluene at $T = 68 \pm 0.1$ °C and quenched at different reaction times. The PMMA concentration is equal to the initial monomer concentration multiplied with the reaction extent (P). The latter was determined using Raman scattering following the procedure explained in reference [19],

and SEC which gave the same results within 5%. We varied the molar ratio R = [EGDMA]/[MMA] between 0 and 0.05 keeping the total monomer concentration constant at 0.26 g/g. Free radical polymerization of MMA ($R = 0$) led to the formation of linear PMMA chains with $M_w = 7.5\times10^4$ g/mol and polydispersity index M_w/M_n=2. We will first discuss in detail results obtained on the system with R = [EGDMA]/[MMA] = 0.01 and subsequently show the effect of varying R.

4.1 Static light scattering (SLS)

Figure 1a shows the q-dependence of I/KC at various reaction extents in a double logarithmic representation. As expected the q-dependence increases with increasing P up to the gel point ($P_c = 0.27 \pm 0.01$). Very close to the gel point a straight line is obtained over the whole accessible q-range:

$$\frac{I}{KC} = 2.54 \times 10^3 q^{-1.67}. \tag{15}$$

When the aggregates are still relatively small M_w and R_{gz} can be determined from the low q-dependence using equations (5, 6). This is no longer feasible if $qR_{gz} > 1$ even for the smallest accessible scattering angle. If the aggregates are fractal and have a power law size distribution then the q-dependence at all P is described by a single structure factor once q is multiplied with R_{gz}, see Section 3. That this is indeed the case for the present system is shown in Figure 1b. The master curve shown in Figure 1b was obtained by simple horizontal and vertical shifts of the curves shown in Figure 1a. As mentioned above the shape of $S_z(q)$ depends on the cut-off functions in equations (1, 2). Klein *et al.* [20] proposed the following empirical expression for $S_z(q)$:

$$S_z(q) = \left[1 + \sum_{i=1}^{n} c_i (qR_{gz})^{2i}\right]^{-\frac{d_f^*}{2n}}. \tag{16}$$

The first and last term in this series expansion are determined by the limiting behaviour at small and large qR_{gz}: $c_1 = (2n)/(3d_f^*)$ and $c_n = a_2^{-2n/d_f^*}$. Using 4 terms equation (16) describes all the data within the experimental error. A non linear least squares fit of the master curve shown in Figure 1b gave $c_2 = 0.976$, $c_3 = 0.376$ and $c_4 = 0.0231$, where we fixed $d_f^* = 1.67$. The limiting q-dependence at large q is given by:

$$S_z(q) = 2.19(qR_g)^{-1.67}. \tag{17}$$

Lines drawn through the data shown in Figure 1a are fits to equations (5, 16) keeping the values of c_i fixed. In this way values of M_w and R_{gz} can be obtained even if equations (5, 6) are no longer applicable.

Figure 2 shows M_w as a function of R_{gz} on a double logarithmic scale. A linear least squares fit gave:

$$M_w = 1.2 \times 10^3 R_{gz}^{1.67}. \tag{18}$$

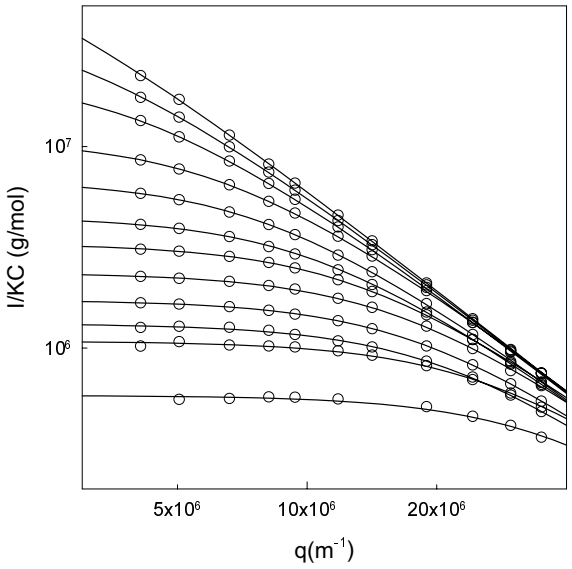

(a)

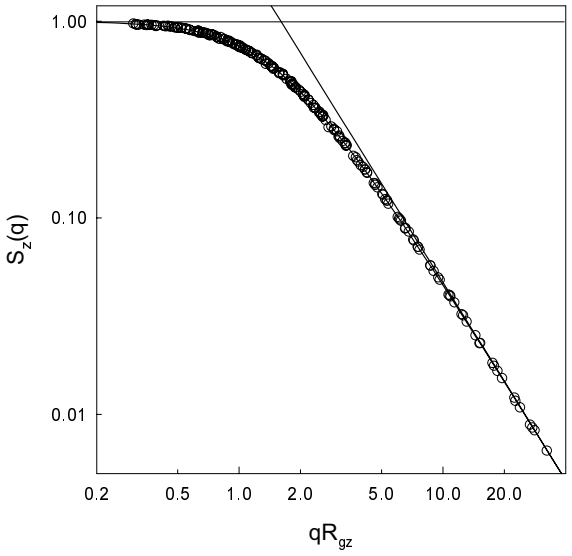

(b)

Fig. 1. (a) q-dependence of the normalized scattering intensity of dilute solutions of PMMA aggregates formed at different reaction extents between 0.18 and 0.27. The solid lines represent fits to a combination of equations (5, 16). (b) Double logarithmic representation of the z-average structure factor of PMMA aggregates. The data are the same as in (a) with I/KC normalized by M_w and q normalized by R_{gz}. The solid line through the data represents a fit to equation (16). The straight line through the data at $qR_{gz} \gg 1$ represents $S_z(q) = 2.19(qR_g)^{-1.67}$.

Thus the same value of d_f^*=1.67 is obtained from the q-dependence of a single system with $qR_{gz} \gg 1$ and from the relation between M_w and R_{gz} obtained for different systems at $qR_{gz} < 1$. The prefactor in equation (18) is consistent with those in equations (15, 17) within the experimental error.

The dependence of R_{gz} on the reaction extent is shown in Figure 3. Monte-Carlo simulations of $3d$ percolation

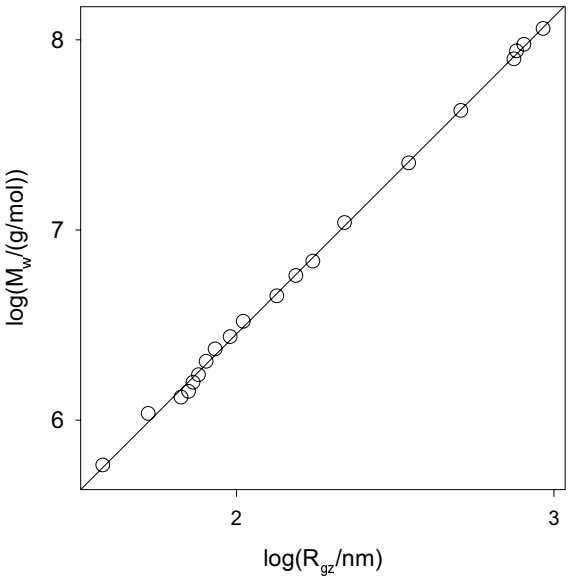

Fig. 2. Double logarithmic representation of the weight average molar mass as a function of the z-average radius of gyration. The solid line represents $M_{\rm w} = 1.2 \times 10^3 R_{\rm gz}^{1.67}$.

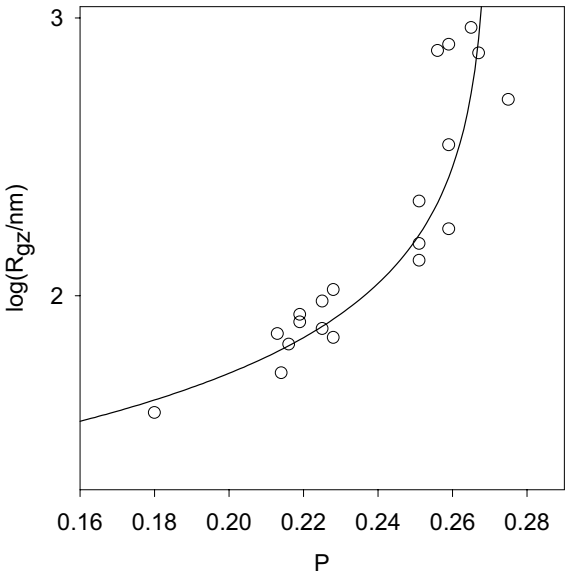

Fig. 3. Variation of $R_{\rm gz}$ with the reaction extent. The solid line represents the expected dependence for percolating clusters: $R_{\rm gz} \propto (P_{\rm c} - P)^{-0.89}$ with $P_{\rm c} = 0.27$.

give $R_{\rm gz} \propto (P_{\rm c} - P)^{-0.89}$ [2]. The line through the data in Figure 3 represents this dependence with $P_{\rm c} = 0.27$. The divergence of $R_{\rm gz}$ at the gel point is compatible with the percolation model. However, an error of 5% on the values of P is too large for this divergence to be a sensitive test of the percolation model.

4.2 Dynamic light scattering (DLS)

Figure 4 shows the normalized electric field autocorrelation functions at different wave vectors for a highly diluted

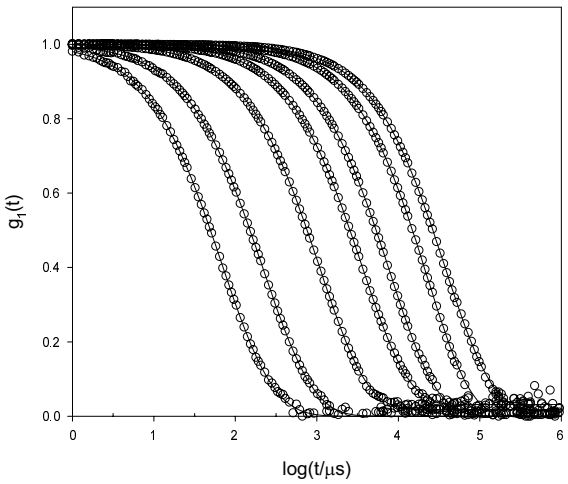

Fig. 4. Normalized electric field autocorrelation functions of dilute solutions of PMMA aggregates formed just before the gel point at different q-values between 4×10^{-3} and 4×10^{-2} nm^{-1} ($13 < \theta < 150$). The solid lines represent fit results (see text).

sample close to the gel point. Small baselines are sometimes observed especially at low scattering angles. These are due to a small number of spurious scatterers in the solutions. The presence of a spurious scatterer is a relatively rare event and it leads to a base line on the measured intensity autocorrelation function. The data were analyzed assuming equation (11) and using the so-called GEX function for the relaxation time distribution:

$$A(\log \tau) = k\tau^p \exp[-(\tau/\tau^*)^s] \tag{19}$$

with k a normalization constant. A detailed discussion of the properties of this function can be found in reference [21]. Note that if we assume $f(M/M^*) = \exp[-(M/M^*)^\beta]$ then comparison of equation (12) with equation (19) gives $p = d_{\rm f}^*$ and $s = \beta d_{\rm f}$ [21].

The lines through the data in Figure 4 show that equation (19) fits the correlograms very well. Using equations (13, 14) we calculated $\langle \Gamma \rangle$ and $\langle \tau \rangle$. The apparent diffusion coefficient was calculated as: $D_{\rm a} = \langle \Gamma \rangle / q^2$. Figure 5a shows the q-dependence of $D_{\rm a}$ at various reaction extents. The q-dependence increases with increasing reaction extent. At large values of $qR_{\rm gz}$, $D_{\rm a}$ increases linearly with q. For self similar systems all curves are expected to superimpose if $D_{\rm a}/D_{\rm z}$ is plotted *versus* $qR_{\rm gz}$. That this is indeed the case is shown in Figure 5b. The master curve is well-described by an empirical expression analogous to equation (16):

$$\frac{D_{\rm a}}{D_{\rm z}} = [1 + 0.652(qR_{\rm gz})^2 + 0.439(qR_{\rm gz})^4 + 0.0324(qR_{\rm gz})^6]^{1/6}. \tag{20}$$

The limiting behaviour at large $qR_{\rm gz}$ is: $D_{\rm a}/D_{\rm z} = 0.57qR_{\rm gz}$. The lines through the data shown in Figure 5a represent non-linear least square fits to equation (20).

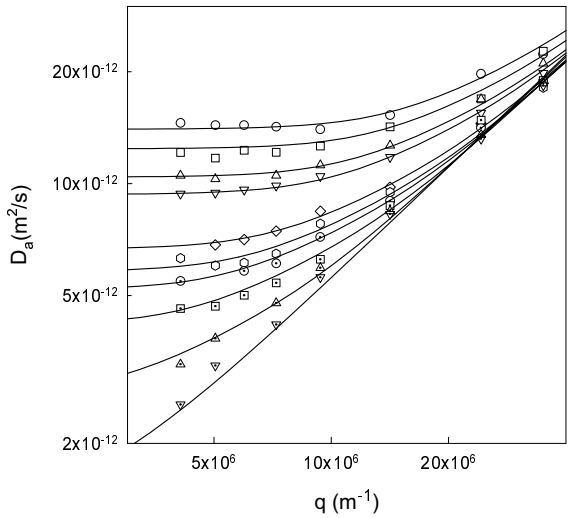

(a)

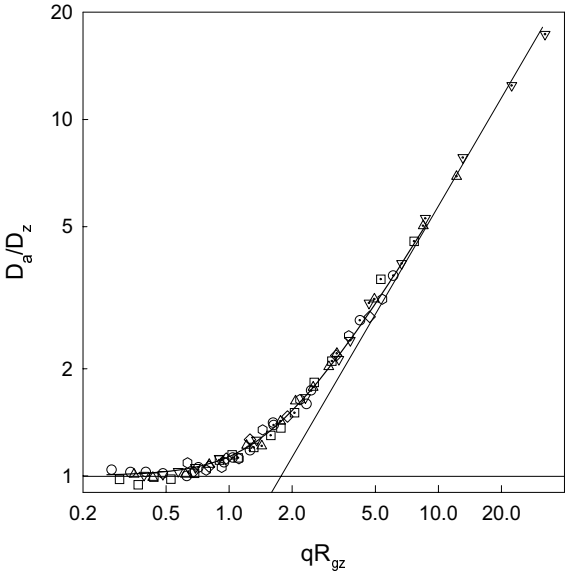

(b)

Fig. 5. (a) q-dependence of the apparent diffusion coefficient $D_\mathrm{a} = \langle \Gamma \rangle / q^2$ of dilute solutions of PMMA aggregates at different reaction extents between 0.18 and 0.27. The solid lines represent fits to equation (20). (b) Same data as in (a) with D_a scaled by D_z and q scaled by R_gz. The solid line through the data represents equation (20). The straight line through the data at $qR_\mathrm{gz} \gg 1$ represents $D_\mathrm{a}/D_\mathrm{z} = 0.57 qR_\mathrm{gz}$.

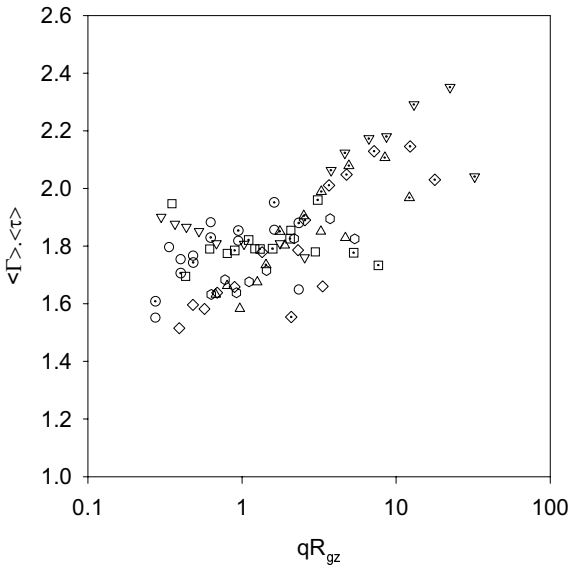

Fig. 6. Dependence of the dynamic polydispersity index $\langle \Gamma \rangle \cdot \langle \tau \rangle$ on qR_gz of dilute solutions of PMMA aggregates at different reaction extents between 0.18 and 0.27.

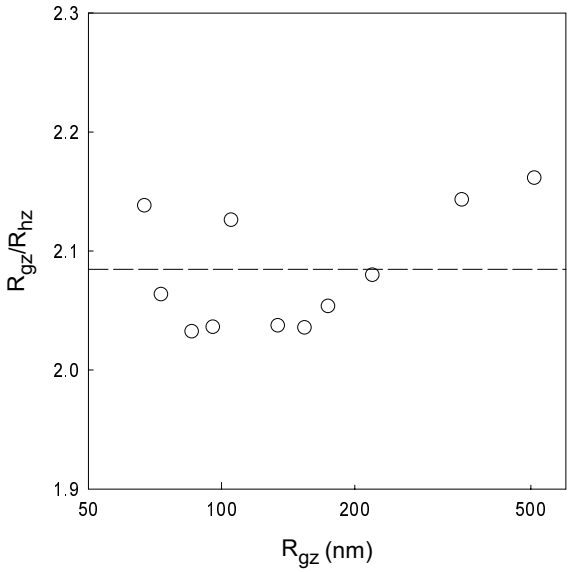

Fig. 7. Variation of $R_\mathrm{gz}/R_\mathrm{hz}$ with R_gz. The mean value is 2.08 and is indicated by the dashed line.

Figure 6 shows $\langle \Gamma \rangle \cdot \langle \tau \rangle$ as a function of qR_gz. The data are noisy because $\langle \tau \rangle$ is very sensitive to the tail of the correlogram and thus to the presence of even a very small amount of spurious scatterers. Nevertheless, it is clear that $\langle \Gamma \rangle \cdot \langle \tau \rangle$ is independent of P which demonstrates the self similarity of the system at different reaction extents. Within the scatter $\langle \Gamma \rangle \cdot \langle \tau \rangle$ is about 1.7 at $qR_\mathrm{gz} < 2$ and increases slightly to about 2.1 at $qR_\mathrm{gz} > 10$. In spite of the scatter of the data it is without doubt that $\langle \Gamma \rangle \cdot \langle \tau \rangle$ does not have a power law dependence on q as expected for rigid percolating clusters [18]. The PMMA aggregates are flexible and at large qR_gz the concentration fluctuations relax mainly due to diffusion of aggregates with a hydrodynamic radius close to q^{-1}.

The z-average hydrodynamic radius (R_hz) was calculated from D_z using equation (10). The ratio $R_\mathrm{gz}/R_\mathrm{hz}$ is shown as a function of R_gz in Figure 7. However, we need to take into account that polydispersity has a different effect on R_gz and R_hz: $R_\mathrm{gz} \propto [\int R_\mathrm{g}^2 M^2 N(M) \mathrm{d}M]^{0.5}$ and $R_\mathrm{hz} \propto [\int R_\mathrm{h}^{-1} M^2 N(M) \mathrm{d}M]^{-1}$. If we want to remove the polydispersity effect we need to compare the same moments of the distribution, *i.e.* we should use $\langle \tau^2 \rangle^{0.5}$ in the calculation of R_hz. If we do this we find $R_\mathrm{g}/R_\mathrm{h} = 1.15$

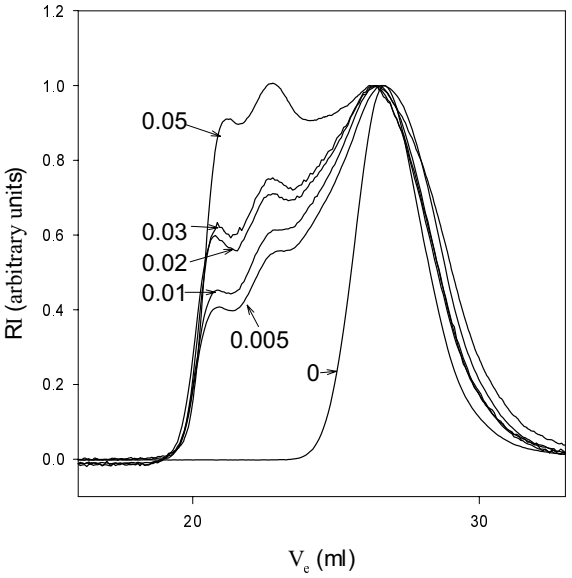

Fig. 8. Chromatograms of PMMA aggregates formed just before the gel point with varying amounts of cross-linker added. The refractive index signal (RI) was measured as a function of the elution volume (V_e). The values of R = [EGDMA]/[MMA] are indicated in the figure. The chromatogram of linear PMMA formed at the same conditions is shown for comparison.

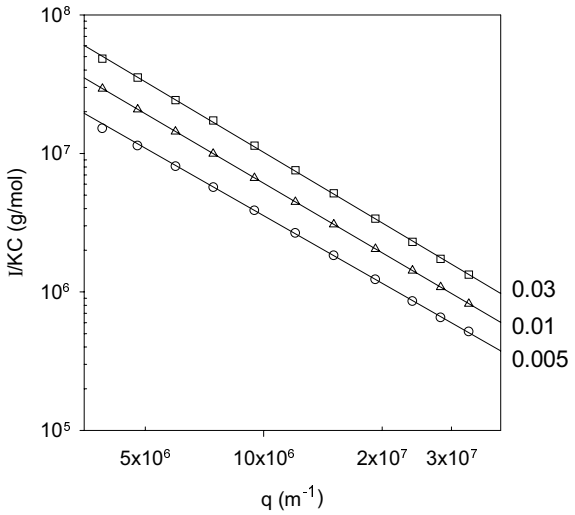

Fig. 9. q-dependence of the normalized scattering intensity of dilute solutions of PMMA aggregates formed just before the gel point with varying amounts of cross-linker added. The values of R = [EGDMA]/[MMA] are indicated in the figure. The solid lines have slopes −1.69, −1.67 and −1.62 for R = 0.03, 0.01 and 0.005, respectively.

instead of $R_{gz}/R_{hz} = 2.08$. Lang *et al.* [22] found $R_{gz}/R_{hz} = 1.1$ for star-branched microgels of PMMA cross-linked with EGDMA and $R_{gz}/R_{hz} = 1.75$ for linear PMMA, both in THF. If we use $R_{gz} = 2.08R_{hz}$ in equation (20) we find that $D_a = (kT/6\pi\eta)1.2q$ for $qR_{gz} \gg 1$, *i.e.* D_a is equal to the diffusion coefficient of particles with $R_h = 0.8q^{-1}$ at large qR_{gz}.

4.3 Influence of the cross-link density

Figure 8 shows chromatograms of solutions quenched close to the gel point containing various amounts of EGDMA. In all cases the maximum is situated close to that of linear PMMA formed at same conditions. The case $R = 0.1$ was treated in detail using online SLS and viscosity detection and the results are reported in [11]. There it was concluded that the data are compatible with a polydispersity exponent τ between 2.1 and 2.2. The swollen fractal dimension was determined from the molar mass dependence of the viscosity and radius of gyration of monodisperse fractions: $d_f = 2.1 \pm 0.1$.

The small hump at the $V_e \approx 21$ on the chromatograms is due to an effect of complete exclusion of the largest aggregates. We do not have an explanation of the hump at $V_e \approx 23$. Such a feature was also observed on other systems [6,8] and could be an artefact of the method. In a first approximation $V_0 - V_e \propto \log(M)$ and therefore the refractive index signal is given by $RI \propto M^2N(M)$, so that the area under the chromatogram is proportional to the total mass injected. The representation of the data in Figure 8 is thus very sensitive to small variations of τ. If $\tau < 2$ then the maximum moves with M^*, while if $\tau > 2$ the maximum stays at M_0. Sometimes the chromatograms are converted to show $\log(N(M))$ *versus* $\log(M)$. Of course, in such a representation small humps on the chromatogram are no longer visible. Figure 8 seems to indicate that τ increases weakly from about 2.2 at $R = 0.005$ to 2.0 at $R = 0.05$. We do not believe, however, that the results from SEC can be used to obtain precise values of τ. The reason is quite simply that $N(M) \propto M^{-\tau}$ is valid only if $M^* \gg M \gg M_0$, else the internal and external cut-off of the distribution influence $N(M)$. The radius of gyration of linear PMMA with $M_w = 7.5{\times}10^4$ g/mol is about 10 nm [22] and aggregates larger than about 50 nm [11] are excluded at the dead volume of the columns. In addition, the external cut-off function of percolating clusters contains a maximum which profoundly influences $N(M)$ at $M < M^*$ and tends to reduce the apparent value of τ. In view of these facts in conjunction with the unexplained hump on the chromatogram it is clear that all we can conclude from SEC is that $N(M)$ does not vary strongly with R (at least for $R < 0.05$) and that $2.0 > \tau > 2.5$.

Figure 9 shows the q-dependence of I/KC of diluted samples close to the gel point at different values of R. The slope and thus d_f^* is the same within the experimental error. However, the intercept increases with increasing R. From SEC we know that the refractive index increment and thus K is independent of R. This means that the local structure is denser with increasing R because a_2 in equation (8) only depends on the local structure if d_f^* is the same. The increase of a_2 with R is most likely due to the increasing density of branching points.

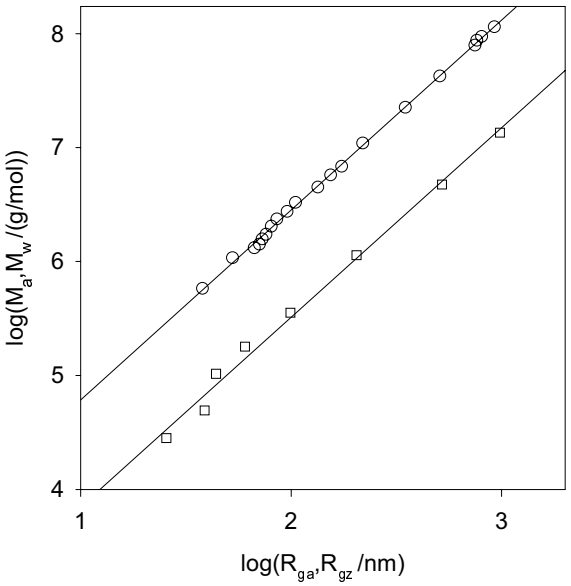

Fig. 10. Double logarithmic representation of the apparent molar mass as a function of the apparent radius of gyration of a solution of PMMA aggregates close to the gel point at different concentrations between 4×10^{-3} and 3×10^{-2} g/ml (squares). The solid line represents $M_\mathrm{a} = 1.53 \times 10^2 R_\mathrm{ga}^{1.66}$. The results on dilute solutions ($M_\mathrm{w} = 1.2 \times 10^3 R_\mathrm{gz}^{1.67}$, see Fig. 2) are included for comparison (circles).

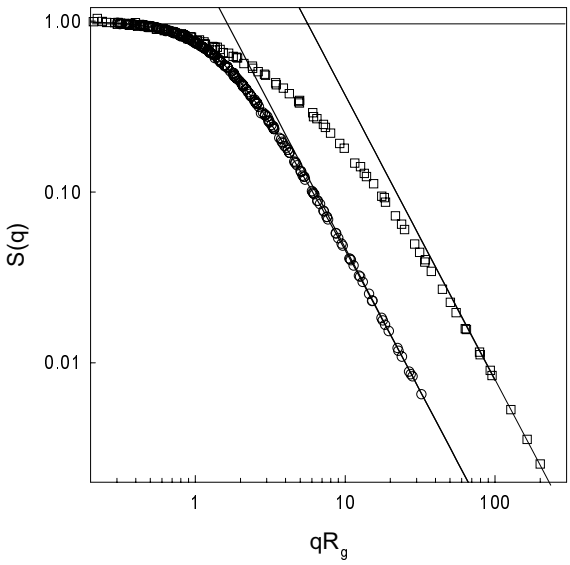

Fig. 11. Comparison of the structure factor of semi-dilute (squares) and dilute (circles) solutions of PMMA aggregates. The straight lines have the same slopes, but the intercepts are +17.2 and +2.19 for semi-dilute and dilute solutions, respectively.

4.4 Comparison with semi-dilute percolating clusters

In reference [10] we have reported results of SLS and DLS measurements on a system prepared close to the gel point and progressively diluted. We have shown that the total scattering intensity and also the q-dependence increases with decreasing concentration. At very high dilution factors a power law dependence was observed over the whole q-range with exponent -1.61.

Daoud and Leibler [23] have proposed a model for semi-dilute solutions of percolating clusters. According to this model the pair correlation function is also given by equation (3) with as sole modification the cut-off function. The cut-off occurs not at R_gz but at the correlation length of the polymer concentration fluctuations (ξ). Of course, $g(r)$ decays to a finite constant value for $r > \xi$ which is given by the average concentration, but for semi-dilute solutions the influence on the scattered intensity is negligible.

In real systems the situation is more complicated because we cannot neglect the scattering from branching points. This leads to two correlation lengths: one characterizing concentration fluctuations of the polymer segments (ξ_p) and another one characterizing concentration fluctuations of the branching points (ξ_b). However, at sufficient dilution ξ becomes much larger than the average distance between branching points so that the system is again characterized by a single correlation length ($\xi = \xi_\mathrm{p} = \xi_\mathrm{b}$).

We can analyze a semi-dilute solution in the same way as a dilute solution in order to obtain an apparent molar mass (M_a) and radius of gyration (R_ga). The latter is proportional to ξ with a proportionality factor of order unity that depends on the cut-off function $f(r/R_\mathrm{ga})$. The structure factor of semi-dilute systems ($S_\mathrm{a}(q)$) can be obtained by superimposing curves determined at different concentrations in a way analogous to that used for dilute solutions at different reaction extents. In reference [10] we showed that the concentration dependence of R_ga is very close to that expected for percolating clusters as already previously observed [24]. Here we compare the structure of the semi-dilute system with that of the dilute system.

At distance scales much smaller than R_ga the structure of a semi-dilute solution is the same as that of a dilute solution. Therefore at $qR_\mathrm{ga} \gg 1$, values of I/KC at a given q are expected to be the same as those for dilute solutions at $qR_\mathrm{gz} \gg 1$, *i.e.* a_2 in equation (8) is expected to be the same. The measured values of a_2 are indeed the same within the experimental error. Figure 10 shows a comparison of M_a as a function of R_ga with M_w as a function of R_gz. A linear least squares fit gave: $M_\mathrm{a} = 1.5 \times 10^2 R_\mathrm{ga}^{1.66}$. The exponent is the same as for M_w as a function of R_gz within the experimental error, but the prefactor is 8 times smaller. Figure 11 shows a comparison of $S_\mathrm{a}(q)$ with $S_z(q)$. The power law dependence is reached at much larger q for $S_\mathrm{a}(q)$. The solid line through the data at large qR_ga represents $S_\mathrm{a}(q) = 17.2(qR_\mathrm{ga})^{-1.67}$. Again the same exponent, but a prefactor that is 8 times larger which demonstrates the consistency of the results.

Comparison of semi-dilute with dilute solutions shows that for semi-dilute solutions d_f^* and a_2 are the same while a_1 is 8 times larger and a_3 is 8 times smaller. These observations are consistent with the idea that the only difference on the pair correlation function is the cut-off function at R_ga and R_gz. The difference of the prefactors a_1 and a_3

implies that the cut-off at R_{ga} in semi-dilute solutions is much more gradual than the one at R_{gz} in dilute solutions.

5 Conclusion

During free radical co-polymerization of MMA with small amounts of EGDMA initially linear PMMA chains are formed. As the polymer concentration approaches the overlap concentration branching, cross-linking leads to the formation of polydisperse aggregates of PMMA chains. The aggregates have a selfsimilar structure and are flexible. The structure and the polydispersity of the aggregates are compatible with those predicted for swollen percolating clusters.

Variation of the cross-link density R = [EGDMA]/[MMA] does not modify the fractal dimension, but the local structure becomes denser with increasing R. SEC shows small changes of the size distribution with R. However, the upper limit of resolution of existing SEC columns is about 50 nm which is too small to obtain accurate estimates of the polydispersity exponent.

The pair correlation function of semi-dilute solutions of the aggregates is the same as that of dilute solutions at distance scales much smaller than ξ and R_{gz}, respectively. The large distance cut-off of $g(r)$ at ξ is more gradual than at R_{gz}.

References

1. D. Stauffer, Chem. Soc. Farad. Trans. II **72**, 1354 (1976); P.-G. de Gennes, J. Phys. **36**, L1 (1976).
2. D. Stauffer, A. Aharony, *Percolation Theory*, 2nd edn. (Taylor & Francis, London, 1992).
3. W.H. Stockmeyer, J. Chem. Phys. **11**, 45 (1943); P.J. Flory, *Principles of Polymer Chemistry* (Cornell University Press, Ithaca, 1953).
4. T. Vicsek, *Fractal Growth Phenomena* (World Scientific, London, 1989).
5. M. Adam, M. Delsanti, J.P. Much, D. Durand, J. Phys. **48** 1809 (1987).
6. E.V. Patton, J.A. Wesson, M. Rubenstein, J.C. Wilson, L.E. Oppenheimer, Macromolec. **22**, 1946 (1989).
7. F. Schosseler, H. Benoit, Z. Grubisic-Gallot, Cl. Strazielle, L. Leibler, Macromolec. **22**, 401 (1989).
8. F. Schosseler, M. Daoud, L. Leibler, J. Phys. France **51**, 2373 (1990).
9. J.E. Martin, D. Adolf, J.P. Wilcoxon, Phys. Rev. Lett. **61**, 2620 (1988); M. Rubinstein, R.H. Colby, J.R. Gillmor, in *Macromolecular Fluids*, edited by F. Tanaka, M. Doi, T. Ohta (Springer-Verlag, Berlin, 1989).
10. V. Lesturgeon, T. Nicolai, D. Durand, Eur. Phys. J. B **9**, 71 (1999).
11. C. Degoulet, T. Nicolai, J.P. Busnel, D. Durand, Macromolec. **28**, 6819 (1995).
12. *Light Scattering from Polymer Solutions*, edited by M.B. Huglin (Academic Press, London and New York, 1972).
13. J. Brandrup, E.H. Immergut, *Polymer Handbook* (Wiley, London, 1975).
14. J.A. Finnigan, D.J. Jacobs, Chem. Phys. Lett. **6**, 141 (1970); E. Moreels, W. De Ceunick, J. Chem. Phys. **86**, 618 (1987).
15. T. Nicolai, D. Durand, J.C. Gimel, Scattering Properties and Modelling of Aggregating and Gelling Systems Light Scattering, in *Principles and Developments*, edited by W. Brown (Clarendon Press, Oxford, 1996).
16. M.E. Cates, J. Phys. Lett. France **46**, 757 (1985).
17. B. Berne, R. Pecora, *Dynamic light scattering* (Wiley, New York, 1976).
18. J.E. Martin, F. Leyvraz, Phys. Rev. A **34**, 2346 (1986).
19. S. Damoun, R. Papin, G. Ripault, M. Rousseau, J.C. Rabadeux, D. Durand, Raman Spectrosc. **23**, 385 (1992).
20. R. Klein, D.A. Weitz, M.Y. Lin, H.M. Lindsay, R.C. Ball, P. Meakin, Progr. Colloid Polym. Sci. **81**, 161 (1990).
21. T. Nicolai, J.C. Gimel, R. Johnsen, J. Phys. II France **6**, 697 (1996).
22. P. Lang, W. Burchard, M.S. Wolfe, H.J. Spinelli, L. Page, Macromolec. **24**, 1306 (1991).
23. M. Daoud, L. Leibler, Macromolec. **21**, 1497 (1988).
24. J.P Munch, M. Delsanti, D. Durand, Europhys. Lett. **18**, 577 (1992).